Rapid Modelling and Control Systems Prototyping of a Marine Robotic Vehicle with Model Uncertainties using xPC Target System

C. S. Chin*, S.H. Lum+
*School of Marine Science and Technology,
University of Newcastle upon Tyne, Newcastle upon Tyne, NE1 7RU
United Kingdom
cheng.chin@ncl.ac.uk

+ School of Engineering
Temasek Polytechnic, Tampines Ave 1, Singapore 529757
Singapore

Abstract: Rapid control systems prototyping have been used to develop controllers for numerous applications. However, most methods are constrained by programming language, embedded systems configurations, and types of operating systems used. These constraints often make the modelling, control systems design and testing difficult to accomplish, and inflexible when dealing with complex mechatronics systems such as an underwater robotic vehicle (URV) before it has been fully developed. With the proposed xPC Target platform, dynamics of the URV including the hydrodynamics parameters can be experimentally determined, simulated and validated easily with computational fluid dynamic method. The experiment with a robust sliding-mode control of the Autonomous Underwater Vehicle (AUV) using the dynamic model obtained is first shown. In the pool trials, the sliding-mode controller deems to be robust enough to control the top control surface angular position despite of the uncertainties in the hydrodynamic parameters obtained and the external disturbance during pool test.

Keywords: modelling, control systems design, mechatronics, underwater robotic vehicles, xPC Target.

1. Introduction

The rapid control systems prototyping have been used to develop controllers for many industry applications. In 1992, a system was developed at Ford [Milam, 1993] to allow the control engineers to use MATLAB/Simulink, to design the controller in graphical form, and generate C code that was then executed in synchronization with a pre-existing embedded controller to allow rapid evaluation of control ideas. Hanselmann (1996) proposed a total development environment, in which the integration among the design of control rules, the system simulation, and the automatic code generation can be accomplished in the same developmental environment. This design concept avoids the integration problem of the conventional control system development, because a series of controller designs and verifications had to be fulfilled in different platforms and environments. With that, a number of rapid prototyping software namely: real-time windows target, real-time embedded target and xPC Target were developed. In 2002, the use of xPC Target was exploited by Burns and Sugar (2002) who applied it to set up a rapid development platform for remote arm control with force feedback in a robotic system. Subsequently in 2007, the real-time workshop (RTW) was used on X–Y table for motion control [Chen et. al., 2007]. For the past two decades, most rapid prototyping of controllers were implemented in the MATLAB/Simulink platform due to its diverse hardware support, complete software solution, and integrated development environment on model based designs without having to write and learn the intricacies of writing detailed embedded code. These can be further seen in the applications such as automotive system design[Loh et al., 2007; Chu et al. 2009, Guo et al., 2009], process control[Saad and Zailani, 2007; Adnan et al., 2010], vibration control[Park et al., 2009; Fei and Yang, 2006] and robotic[Low et al., 2005; Wei et al., 2005] systems.

As observed from the above-mentioned literatures, the prototyping of the embedded system could vary according to applications. Noticeably, it has not covered much on the underwater robotic vehicles (URV) such as an autonomous underwater vehicle (AUV) [Chin et al., 2009] development using xPC Target, in particular, the rapid control system prototyping involving dynamic modelling, control systems design, hardware-in-the-loop testing and implementation. Besides, most underwater robotic systems development [Fehrani et al., 2010; Byron and Tyce, 2007], just to name a few, used QNX, Unix-OS/90, LinuxMZ

runtime environment in their control systems design. These methods may not be easy for engineers and/or students to use as it consists of extensively C/C++ programming codes and inputs-outputs circuitry for interfacing prior to the dynamics modelling, and also the testing of the hydrodynamic parameters for the control systems design. In recent years, there has been much interest in the development of AUV and the practical application of AUVs that involves major challenges of precise track-keeping and fast obstacle avoidance [Ura at al., 2006]. Recently, AUV development capacity is enhanced by the use of the computational modelling in the design, manipulation, and control of AUVs. The use of xPC Target computer models provide a means of modelling and determining the performance of a proposed vehicle during the design phase, and to devise and optimize a controller for enhancing the vehicle's performance characteristics iteratively using hardware-in-the-loop concept.

To facilitate the dynamic modelling and subsequent motion control of the AUV with the installed thrusters, the works are broken down into three sub-tasks: the determination of the hydrodynamic coefficients of the vehicle, the simulation of the control systems design, for a known set of control inputs, to obtain the ensuing motion of the vehicle, and the testing of the AUV in the field. The uncertainty involved in the determination of the hydrodynamic coefficients usually induces the errors in the model or final result. However with robust control scheme [Utkin, 1977] that has the ability to compensate for these modelling errors and uncertainties, the accuracy of the hydrodynamic coefficients would not pose a great problem in most URV control systems design. The main contribution of the paper is the integration of xPC-Target in a systematic approach from the modelling and simulation to the subsequent control system design on the AUV before and during the actual implementation. Hence, the proposed systematic approaches felicitate the designing and testing of a typical marine vehicle such as the AUV system.

The paper is organized as follows. The paper is organized as follows. In Section 2, the essential hardware and software used in conjunction with xPC Target are introduced. In Section 3 and 4, the modeling of the AUV dynamics in horizontal plane and the actuator dynamics are shown respectively. In Section 5, the hydrodynamics modeling of the AUV is discussed. It is followed by the sliding-mode control system design for controlling the top control surface angular position in Section 6. Lastly, the obstacle avoidance test in the pool is shown in Section 7, and the paper is concluded with future works.

2. AUV and xPC Target System Overview

An autonomous underwater vehicle (AUV) was constructed in 2009 to serve as a test-bed for systems research, and as a general research and development tool for years to come. It is neutrally buoyant in water, axi-symmetric and has a cylindrical-like body as shown in Fig.1. The vehicle has an overall length (L) of 0.6 m, a diameter (D_a) of 0.25m and a dry weight (m) of approximately 14 kg. The center of buoyancy is located at (0, 0, -0.001m). The thruster is made up of a brush-type DC motor and a three-bladed propeller (with diameter equal to 0.18m). The AUV has a pair of side fins and a pair of top and bottom control surfaces near its end part generates yawing moments for horizontal movement. The necessary power is supplied by packs of lithium ion batteries, which can be sustained to operate at a speed of maximum 1m/s for 3 hours. The vehicle is equipped with an altimeter sensor for measuring forward distance and a magnetic compass for measuring heading. The encoders at the motors are for measuring the angular position and the angular velocity of the motor shaft.

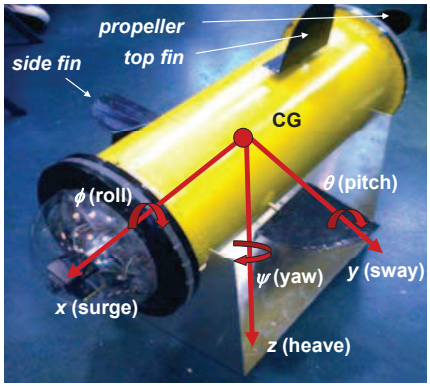

Fig. 1: A test-bed AUV with coordinate systems

For AUV modelling and control verification using the hardware-in-the-loop concept, the xPC Target software and hardware as shown in Fig. 2 are used. The schematic diagram of system setup composed of:

- an industrial PC104- Athena II CPU (or Prometheus CPU) card,

- a Pandora enclosure with DAQ card,
- two brush-type Transmotec DC motor with encoder,
- a three-bladed propeller,
- four Omega strain gages with Kyowa amplifier,
- two Advanced power amplifiers,
- a Honeywell magnetic compass, and
- a Tritech PA200 digital precision altimeter.

The motion of the vehicle is controlled by an onboard industrial PC104 computer in target PC, which runs with the help of the xPC Target software and Target kernel. Ethernet link is used for communication with the host PC that has MATLAB and Simulink packages installed. The PC104 computer, Athena II is connected to power amplifier, DC motor, altimeter and magnetic compass. When the executable code is running in xPC Target kernel, the commanded voltage signals are generated from the I/O board analog output channels and go into the power amplifiers to drive the respective DC motors. As shown in Fig. 2, the encoders are connected to digital channel of the I/O board whilst the altimeter is connected to the analog input of the I/O board. The magnetic compass is connected to the RS232 port and was calibrated against the software as shown in Fig. 3. To operate and test the test-bed AUV, the Simulink block diagram that contains the proposed control system design is compiled (using Microsoft Visual Studio V9.0 complier) and then downloaded to the target PC that runs the highly optimized xPC Target kernel. For real-time monitoring and analysis, the Ethernet link allows the model parameters and command inputs to be changed whilst the AUV is running. For standalone control or during the actual test in water, the Ethernet cable could be disconnected from the target PC and the data collected can be retrieved later for analysis

Figure 2 shows the use of xPC Target to systematically link the modelling and simulation to the control system design (using sliding mode controller) on the AUV before and during the actual implementation. The modelling involved obtaining the thruster dynamic, hydrodynamic forces and moment damping coefficients from the measured 3 degrees of freedom (DOF) motion data of the AUV using an open-tank test and ANSYS CFX. The hydrodynamic added mass coefficients were determined analytically using the strip theory. From the measured position and velocities data, the AUV model was compared with the simulated results from the MATLAB/Simulink. The process repeats until the output data matches the simulated results within a reasonable bound. After the open-loop AUV dynamics model was obtained, the sliding-mode controller was then designed to control the angular position of the top control surface while the proportional-integral-derivative (PID) controller was used to control the propeller angular speed. As seen in Fig. 2, to verify the overall control systems design and the hydrodynamic coefficients obtained from the experiment and the CFD simulation, the AUV was conducted in a swimming pool.

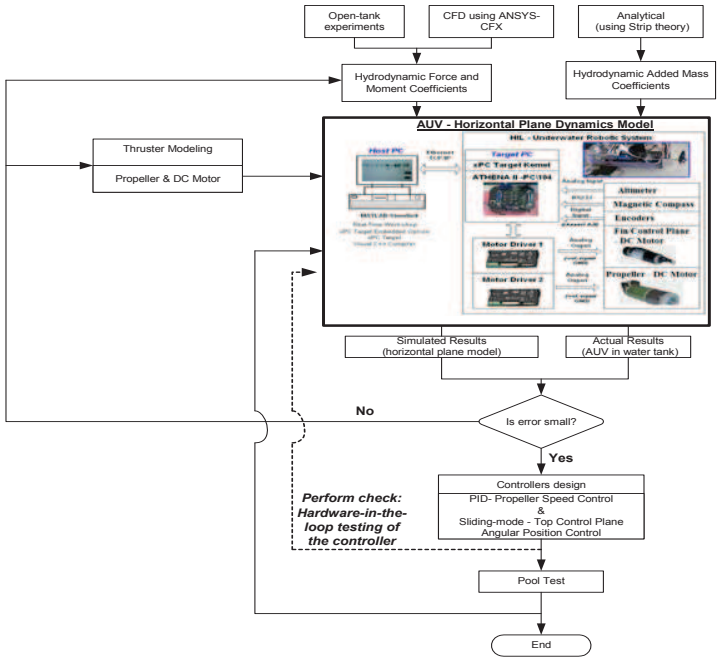

Fig. 2: Rapid control system prototyping process flow for test-bed AUV

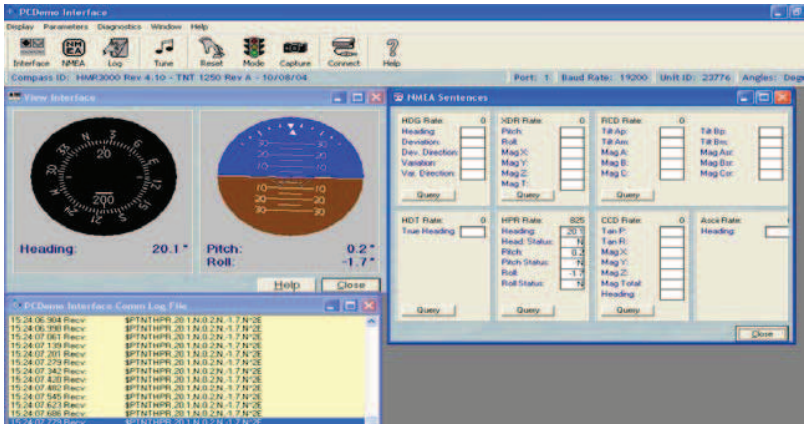

Fig. 3: PC interface program for magnetic compass

3. AUV Dynamic Model

Considering the coordinate systems shown in Fig. 1, the body-fixed frame coincides with the principle axes of the vehicle and is free to translate and rotate with respect to the Earth-fixed frame. The origin of the body-fixed frame is the center of mass of AUV. The positive x axis is oriented in the forward direction of the vehicle along the longitudinal centerline and the positive z axis is oriented downwards.

The rigid body URV dynamic equation is commonly expressed in the body-fixed frame since the control forces and measurement devices are easily and intuitively related to this body frame of reference. Using the Newtonian approach, the motion of a rigid body with respect to the body-fixed reference frame at the origin can be obtained. A detailed discussion about the AUV modelling was presented in [Fossen, 2002] and the hydrodynamic forces and moments modelling could be found in [Gertler and Hagen, 1967; Lamb, 1932]. The main assumptions made in deriving the URV's dynamic equation are namely: (a) the vehicle is a rigid body and is fully submerged once in water; (b) the vehicle is slow moving for operation in underwater; (c) The earth-fixed frame of reference is inertial. In equation (1), the external force and moment vector includes the hydrodynamic forces and moments due to damping, inertial of surrounding fluid, the restoring force and moment. These forces and moments tend to oppose the motion of the AUV. The equations of motion can be described by a set of six differential equations in the body-fixed frame as follows:

$$\mathbf{M}\dot{\boldsymbol{\nu}} + \mathbf{C}(\boldsymbol{\nu})\boldsymbol{\nu} + \mathbf{D}(\boldsymbol{\nu})\boldsymbol{\nu} + \mathbf{G}(\boldsymbol{\eta}) = \boldsymbol{\tau} \tag{1}$$

where $\boldsymbol{\nu} = [u \quad v \quad w \quad p \quad q \quad r]^{\mathrm{T}}$ is the body-fixed velocity vector, $\boldsymbol{\eta} = [x \quad y \quad z \quad \phi \quad \theta \quad \psi]^{\mathrm{T}}$ is the earth-fixed vector that comprises the position and the Euler angles. $\mathbf{M} \in \Re^{6\times6}$ is the sum of the rigid body and added inertia mass matrix. $\mathbf{C}(\boldsymbol{\nu}) \in \Re^{6\times6}$ is the sum of rigid body and added mass Coriolis and centripetal forces and moments matrix. $\mathbf{D}(\boldsymbol{\nu}) \in \Re^{6\times6}$ is the damping matrix due to the surrounding fluid and $\boldsymbol{\tau} \in \Re^{6}$ is the input force and moment vector from the actuator and control surface.

As observed in the URV dynamics in (1), it is highly-coupled and nonlinear in motions. In most AUV design, they are designed for horizontal and/or vertical [Byron and Tyce, 2007; Fossen, 2002] plane motion. This reduces the coupling in motions as the AUV move in one plane at a time. Most AUVs adopt a decoupled maneuver scheme: moving with a horizontal plane motion whereby the vehicle is first steered at constant forward speed along a straight line to a desired target point. Thus considering only few DOF at a time decouples the motions. It also reduces the number of controllable DOF in subsequent control systems design. In the test-bed AUV, it is designed to operate in the horizontal plane with a constant heave. The horizontal plane dynamic used in the AUV can be written as:

$$(m - X_{\dot{u}})\dot{u} + X_{|u|u}|u|u + (Y_{\dot{v}} - m)vr = \tau_{xt} \tag{2a}$$

$$(m - Y_{\dot{v}})\dot{v} + Y_{|v|v}|v|v + (m - X_{\dot{u}})ur = \tau_{yt} \tag{2b}$$

$$(I_z - N_{\dot{r}})\dot{r} + N_{|r|r}|r|r + (-Y_{\dot{v}}u + X_{\dot{u}}u)v = \tau_{\psi t} \tag{2c}$$

where $\tau_{xt}, \tau_{yt}, \tau_{\psi t}$ are the input forces and moment. $X_{\dot{u}}, Y_{\dot{v}}, N_{\dot{r}}$ are the hydrodynamic added mass coefficients. $X_{|u|u}, Y_{|v|v}, N_{|r|r}$ are the nonlinear hydrodynamic damping coefficients. The AUV mass, *m* is around 14 kg and the inertia about Z-axis was computed using the software Pro/ENGINEER. The moment of inertia, I_r was found to be 0.093 kg.m^2.

A number of methods have been proposed to determine the hydrodynamic coefficients. They can be broadly broken down into test-based and predictive methods. Test-based methods involve experimental determination of the hydrodynamic parameters directly based on towing-tank model tests, as well as the testing of full-sized vehicles [Aage and Wagner, 1994; Yoon et al., 2007; Yoon and Son, 2004]. One disadvantage of the above methods is the need for an accurate physical model of the vehicle or the vehicle itself, as well as laboratory or in-field testing facilities. These are often not available, either for reasons of cost or simply due the vehicle has not yet been constructed.

Predictive methods offer an attractive alternative to test based methods when the vehicle is still in the design stages or when cost prohibits a full-scale testing program. The most basic of the predictive methods are purely analytical methods, but these are prone to yielding unrealistic results for complex bluff bodies. Jones et al. (2002) provided a detailed discussion and evaluation of three of the existing methods. Empirical and semi-empirical methods are the most widely used of the predictive methods and have been shown to yield reasonable results [Nahon, 1993; Humphreys, 1981; Kim et al., 2002a, 2002b]. The above predictive methods are likely to yield reasonable results on a streamlined vehicle since their dynamics are more easily predicted.

Since the AUV is not a complex block structure, suggesting that a less complete approach may be required to quantify the hydrodynamic coefficients. An alternative semi-predictive approach that uses the CFD and test method was used. This method is becoming increasingly tractable due to the development of CFD packages and the xPC Target to facilitate the real-time data collection of the parameters from the tank test. However, in any methods used, it will always subject to experimental and numerical errors. Thus, due to these error or uncertainties, the model derived by either method has to depend on some form of robust control scheme such as the sliding-mode control (as seen in later section) to control the AUV.

As shown in the dynamic equations in (2), the hydrodynamic added mass and damping coefficients are the unknown and need to be determined. In this study, three groups of experiments were performed. They are namely: (a) thruster experiments to obtain the steady-state thruster's dynamics in Section 4; (b) steady motion experiments with the AUV to acquire the curves of the forces and moments versus the velocity variables and to verify the validity of CFD simulation using similar approaches; (c) constant thrust tests to verify the values of hydrodynamic coefficients acquired by the CFD, semi-empirical formulae and experiment tests method in Section 5; (d) and final testing of the proposed sliding mode controller in the pool in Section 7.

4. Steady-State Thruster's Dynamics

The thruster consists of a DC motor connected to a three-bladed propeller. To determine the thrust developed by the thruster at different voltage input, the dynamics of the thruster need to be studied. As shown below, the dynamics of the DC motor is obtained followed by the propeller's dynamics. Through experiment, it was observed that thruster's dynamics at low speed can be modeled as a simple linear function of the propeller's thrust and the input voltage whilst the propeller angular speed can be obtained via the steady-state DC motor model. Here, we briefly discuss the model and how it was incorporated in the simulation.

$$J_m\dot{\Omega} + \frac{K_m K_e}{R_m}\Omega = \frac{K_m}{R_m}\bar{u} - Q \tag{3}$$

$$\bar{u} = R_m I_t + L_m \frac{dI_t}{dt} + K_e\Omega \tag{4}$$

where $\bar{u}$ is the voltage input to thruster in V, R_m is the armature resistance in Ohms, I_t is the current to the armature in Ampere, L_m is the inductance in Henry, K_m is the motor torque constant N.m/A, K_e is the motor back emf in V.s/rad, J_m is the rotor moment of inertia in Nm.s^2/rad, Ω is the rotational speed of the propeller in rad/s, Q is the propeller's torque in N.m. The propeller's thrust model [Whitcomb and Yoerger, 1999; Yoerger, 1990] at steady-state (without considering the axial fluid velocity at propeller) can be obtained using the following equation:

$$\tau_x = K_{Td}\Omega^2 \tag{5}$$

τ_x is the thrust from the propeller in N and K_{Td} is the thrust constant in N.s/rad.

Note that, the thrust equation in (5) is usually a function of control surface angle (φ), forward speed, propeller diameter and aspect ratio (that is the ratio between the screw diameter and the height of the fin). However, assuming the fin's deflection is small and the resistance due to the fin's deflection at low speed is negligible (since the fin is mounted at a distance away from the propeller), the effective thrust can be approximated as:

$$\tau_{xt} \approx (1-t_d)\tau_x = (1-t_d)K_{td}\Omega^2 \tag{6}$$

From the experiment in the water tank, an approximated linear relationship between the thrust, and the commanded voltage input for the thruster was obtained. The AUV was tested at a slow forward speed due to the space limitation of the tank (10m×10m×2m) as shown in Fig. 4. The AUV platform in Fig. 1 was concealed using a water-tight aluminum casing. The torque was measured using series of strain gages attached to the motor shaft, and the calibration was executed in air with known masses. The test results showed linear behavior according to mass variations. The readings from the torque sensor were obtained via the interface connected to the computer. The applied voltage to the thruster was measured using a digital oscilloscope. The experiments were repeated a few times to ensure the results were consistent. After the experiments, the thrusts were stored and computed offline by dividing the torque values from the strain gages by the pitch radius of the propeller. The experimental plot for the thrusts vs the applied voltage was then plotted as shown in Fig. 5. The plot gives a reasonable correlation between the thrust and the voltage as the correlation factor falls in the typical range of 0.7 to 1. With the experimental results, the thrust and the voltage input relationship can be written as:

$$\tau_{xt} \approx f_T \bar{\mathrm{u}} \tag{7a}$$

where $f_T = 4.03\mathrm{N/V}$.

The above relationship implies that the thrust is directly proportional to the voltage. As the input to the thruster is in voltage, it makes sense as the voltage increases proportionally with the speed (and the thrust). Therefore, the force in the subsequent sway and yaw direction can be written as:

$$\tau_{yt} = \tau_{xt} \sin\varphi \tag{7b}$$

$$\tau_{\psi t} = L/2\ \tau_{xt} \sin\varphi \tag{7c}$$

where φ is the angle of the top control surface and L is the length of the AUV.

By manipulating the equations in (7) into matrix form, it becomes:

$$\begin{bmatrix} \tau_{xt} \\ \tau_{yt} \\ \tau_{\psi t} \end{bmatrix} = f_T \overbrace{\begin{bmatrix} 1 & 0 & 0 \\ 0 & \sin\varphi & 0 \\ 0 & 0 & L/2.\sin\varphi \end{bmatrix}}^{\mathbf{T}} \bar{\mathrm{u}} \tag{8}$$

where $\mathbf{T}$ is the thrust configuration matrix.

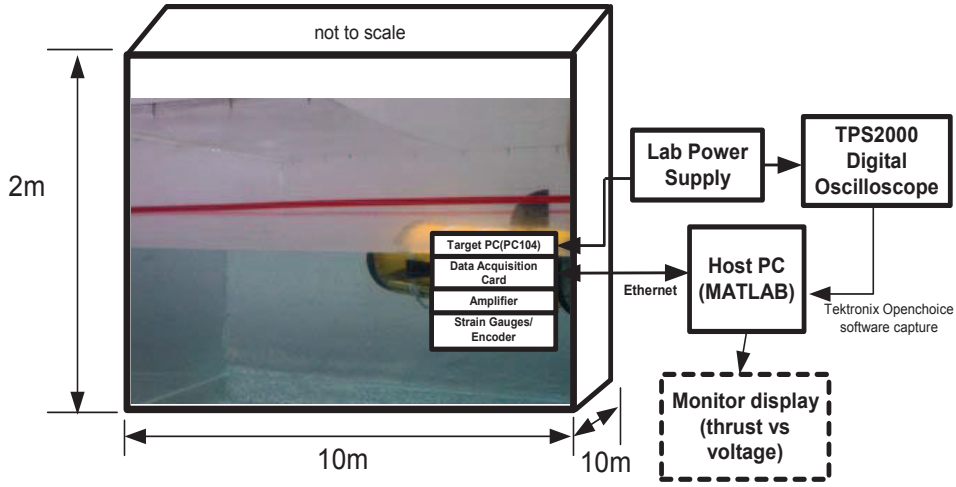

Fig. 4: Tank experiment measuring thrust and voltage input of thruster

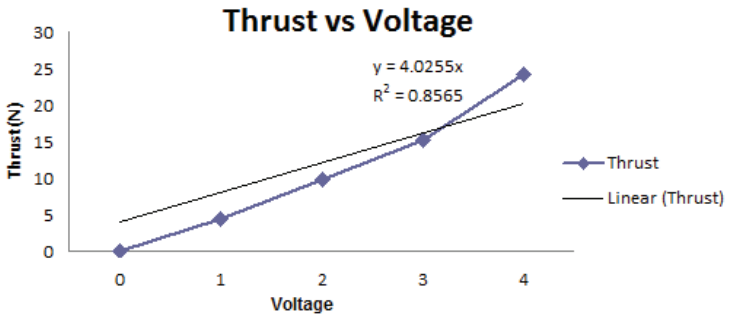

Fig. 5: Thrust vs voltage input to a thruster (forward motion)

The time responses of the thrusts were also captured during the experiment. Due to the tank size, the AUV was left running for only 8s before it reached the other side of the tank. The results shown the thrusts are able to settle to the steady-state values and the settling time is around 2s for different voltage inputs. The xPC Target hardware and simulation model as shown in Fig. 6 were used to obtain the relationship between the angular speed of the propeller shaft and the input voltage. The speed was captured via the encoder mounted on the motor and the voltage was supplied by the laboratory DC power supply. With the speed and input voltage relationship obtained, xPC Target model was used to compare the actual measurement results with the xPC Target simulated data. The angular speeds were computed using the motor's encoder that has 24 counts (for each leading edge transition) per revolution (CPR) for the 2 channels together. As observed in the xPC Target, it is useful to control the propeller's angular speed via the input voltage to the thruster. For small electrical inductance, the open-loop transfer function for the speed $\Omega(s)$ over the input voltage $\overline{u}(s)$, is modeled as a first order system with process delay (that is time delay=1s, time constant=0.01s and motor gain = 0.028). By comparing the simulated result with the actual test (at a certain voltage input) in Fig. 7, there is a good match in the steady state except for the slight deviation during the transient stage. However, the different is quite negligible.

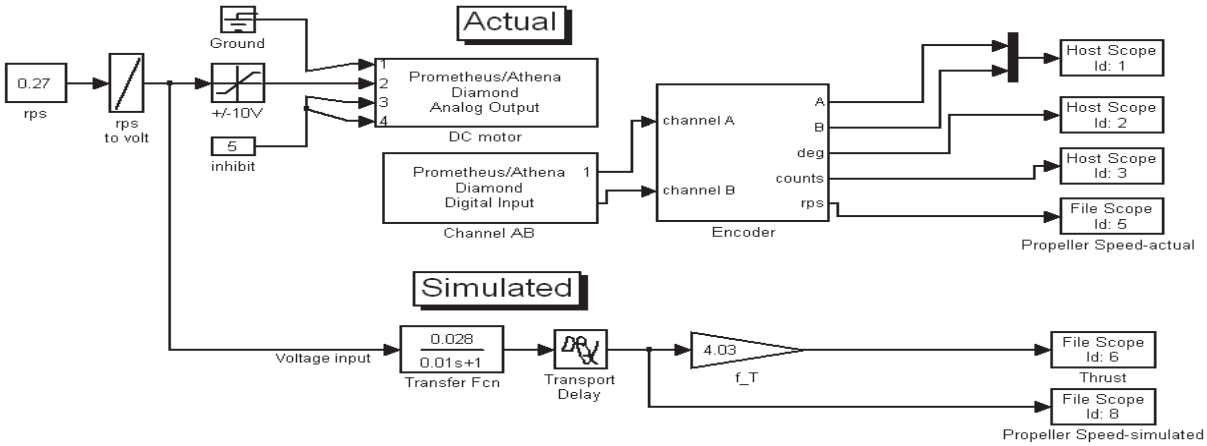

Figure 6: xPC Target block diagram to determine propeller's speed vs input voltage

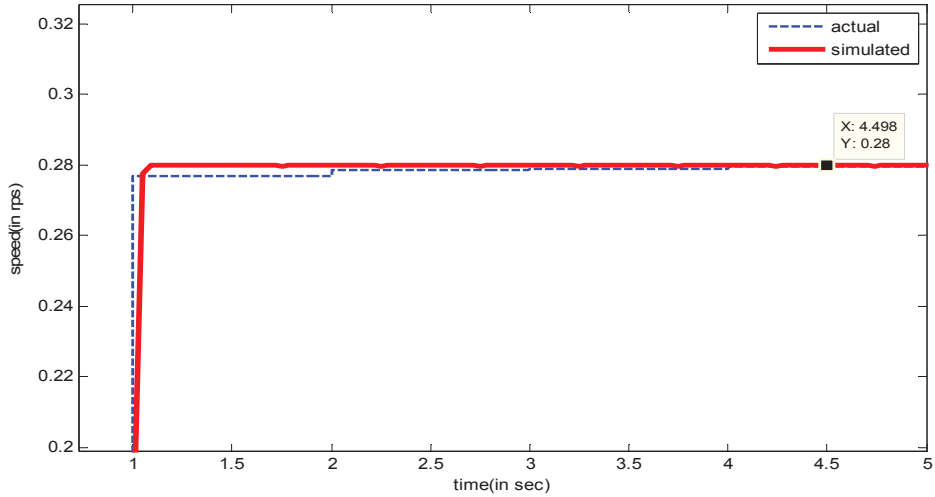

Figure 7: Simulated and actual propeller's speed over time in water tank test

5. Hydrodynamic Forces of AUV

This section determines the hydrodynamic added mass and damping coefficients of the AUV that were computed offline. In the AUV, the resultant flow field is mainly a function of the Reynolds number of the vehicle. The Reynolds number of a rigid body is the ratio of the inertial effects to the viscous effects within the fluid. The Reynolds number of the AUV was computed to be 6×10^5.

The added mass coefficients which arise is due to potential flow phenomena for acceleration in translation and rotation, and the other is the damping coefficients which is due to viscous phenomena for translation and rotation of the body. In most streamlined AUV design, the added mass coefficients $X_{\dot{u}}, Y_{\dot{v}}, N_{\dot{r}}$ are computed analytically using principle of Strip theory [Fossen, 2002]. It involves dividing the submerged part of the vehicle into a number of strips. The two-dimensional hydrodynamic coefficients for the added mass can be computed for each strip and summarized over the length of the body to yield three-dimensional coefficients. In this study, the AUV is considered as a slender body. The added mass coefficients for

each direction can be analytically computed. By substituting the values into the equations [Fossen, 2002], the approximate added mass coefficients for each directions are obtained as: $X_{\dot{u}} = 1.4$, $Y_{\dot{v}} = 29.4$ and $N_{\dot{r}} = 0.1$.

As seen in Fig. 8, another set of experiments were carried out in the 10 × 10 × 2-m open tank (tank is not shown for clarity) to investigate the motion characteristics of the AUV in surge, sway, and yaw in the positive direction on the horizontal plane. Each experiment was repeated a number of times at each velocity and the average damping force readings (the longitudinal force $X_{|u|u}$, the transverse force $Y_{|v|v}$ and moment $N_{|r|r}$ are the surge force, sway force and yaw moment respectively) were tabulated in Table 1. With the vehicle surge or sway set to a constant velocity, the thrust can be considered to be equal to the hydrodynamic force, and the moments provided by thrusters can be considered to be equal to the hydrodynamic moments when it yaws at a constant angular velocity. Hence, the data in Table 1 of the thrust versus the motion variables are assumed to be same as the curves of hydrodynamic loads versus these velocity variables.

The test equipment consists of a DWT draw-wire displacement transducer (string pot) that was used to measure the displacement of the vehicle in water with respect to time. The terminal velocities of the vehicle were determined. The AUV was orientated such that the displacement in each direction can be measured during the test. For example, Fig. 8 shows the testing of the damping force in X direction. To measure the damping force in Y direction, the AUV has to rotate 90 degrees (clockwise) so that the lateral side faces the longitudinal direction. The torque sensor (or pre-wired strain gage) mounted on the motor shaft measured the torque generated and later converted to the translational force in the AUV's X and Y direction. The pre-wired strain gages on the beam surfaces captured the moment generated during the yaw motion (moment about Z axis). The net forces and moments to move the AUV were then determined.

To save the computational cost, the equations of motion can be simplified based on the assumptions: (a) the vehicle moves only along the direction of thrust, (b) the hydrodynamic moment is negligible, and (c) the attitude angles or the pitch angle are always zero. The vehicle is moving linearly in each direction and the maximum speeds at each direction (that correspond to zero acceleration) were measured. The damping coefficients in X and Y direction were determined. For drag force in X and Y direction are $X_{|u|u} = \tau_x / u_{\max}^2$ and $Y_{|v|v} = \tau_y / v_{\max}^2$ respectively. For drag force about Z-axis, the AUV was allowed to rotate freely so that the top control surface could change the AUV's heading direction. Assuming maximum displacement (or zero velocity) in X and Y direction, the thrust becomes: $N_{|r|r} = \tau_\psi / r_{\max}^2$.

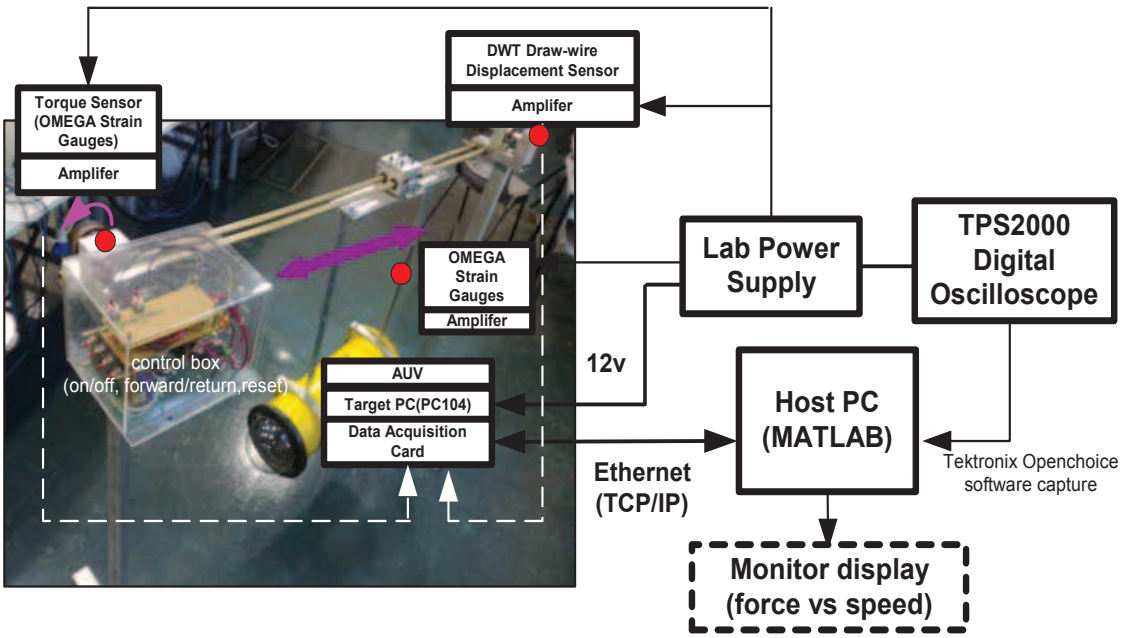

Fig. 8: Rig for drag testing in X direction (water tank not shown for clarity)

The estimated damping coefficients of the AUV have a velocity range from 0 to 0.95m/s (at an increment of 0.1m/s) and the values of the experiment results can be seen in Table 1 while the curves of the thrust vs the motion variables (u, v, r) are shown in Fig. 9. Before much conclusion can be made, the experiment results obtained from the water-tank test were compared with CFD simulation using ANSYS-CFX.

Velocity (m/s)	Experiment (L/D=2.5)			Present ANSYS-CFX (L/D=2.5)		
	$X_{\|u\|u}$ (Ns^2/m^2)	$Y_{\|v\|v}$ (Ns^2/m^2)	$N_{\|r\|r}$ (Ns^2/rad^2)	$X_{\|u\|u}$ (Ns^2/m^2)	$Y_{\|v\|v}$ (Ns^2/m^2)	$N_{\|r\|r}$ (Ns^2/rad^2)
0	0	0	0	0	0	0
0.1	0.62	0.81	0.45	0.52	0.51	0.35
0.2	0.71	0.95	0.98	0.61	0.75	0.78
0.3	0.85	1.19	1.21	0.75	1.04	1.01
0.4	0.83	1.21	1.23	0.78	1.11	1.13
0.5	0.86	1.21	1.29	0.76	1.15	1.18
0.6	0.88	1.24	1.35	0.84	1.19	1.23
0.7	0.91	1.25	1.28	0.87	1.21	1.25
0.8	0.91	1.32	1.29	0.94	1.26	1.26
0.95	0.92	1.34	1.32	0.93	1.31	1.3
Grand Average	**0.75**	**1.05**	**1.04**	**0.70**	**0.95**	**0.95**
Non-dimensional results [Tyagi and Sen, 2006] on Kempf model (using ANSYS-FLUENT, L/D=6)				Not available	**0.0767**	**0.0185**
Present Non-dimensional results on Kempf model (using ANSYS-CFX, L/D=6)				Not available	**0.0811 (5.7% error)**	**0.0192 (3.8% error)**

Table 1: Comparison between experiment and ANSYS-CFX nonlinear damping coefficients for AUV

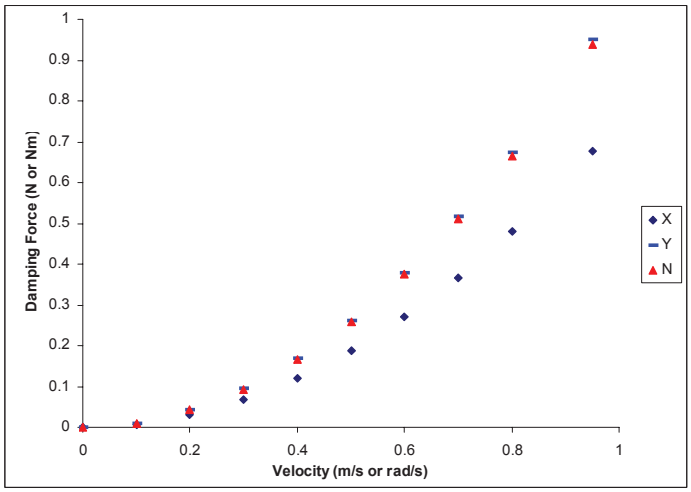

Figure 9: Nonlinear damping force in X, Y and moment about Z from experiment

There are a few pre-processing steps required to be performed before the CFD simulation. In ANSYS-CFX, the flow domain was divided into three regions: a boundary layer region, the space closely around the vehicle and the outer region. All three regions included only tetrahedral elements, the size of which was increased from the vehicle surface to the outer region. First, we determined the distance from the wall to the first grid point or the y+ value. In practice, we don't resolve the solutions of turbulent flow by direct numerical simulation. This should only be used if the mesh is fine enough to resolve the viscous sub-

layer. If y+ values substantially exceed 1, significant errors will result. For the free stream velocity of 1m/s at 20^{o}C water and 0.6m of boundary layer length, the estimated y+ is around 0.0088mm.

To minimize the number of elements, an irregular small mesh was applied only to a small region near the vehicle. In this small region, we specify that the mesh is composed primarily of tetrahedral elements; in this way, around 376,488 irregular elements were built with 72681 nodes. The outer region is a rectangular volume. Its length is 20 times the vehicle length and the height is 5 times greater than the vehicle diameter. In total, around 803,262 elements were built. The region of disturbed flow (usually turbulent) downstream of the AUV body moving through a fluid, caused by the flow of the fluid around the body is formed as shown in the streamlines plot in Fig. 10. The region creates high velocity (or low pressure) region at the rear end and thus low velocity (or high pressure) in the front resist the vehicle motion.

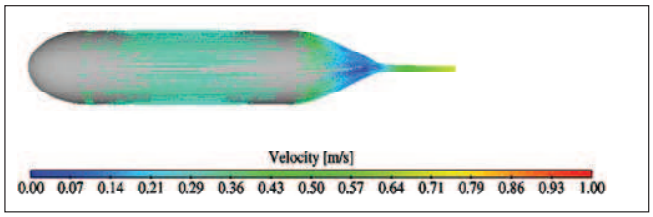

Fig.10: Streamlines plot of AUV

In ANSYS-CFX, the flow in the domain surrounding the vehicle was simulated for various speeds ranging from 0 to 0.95m/s (see Table 1). The hydrodynamic loads or the damping forces were obtained by integrating the pressure on its surface, which was obtained via the simulation. As observed in Table 1, the forces show good agreement when the vehicle surges and sways however, the calculated moments are smaller than the experimental results. There are two main reasons for the differences in the moments. The first is that the thruster is not considered in the CFD model, which may lead to an error in the simulated hydrodynamic center of rotation. The other is that some small changes were made to adjust the center of gravity and buoyancy in the experiments due to the fixture that held the AUV during the test, which implies that they may be different from their design points. Both of these factors have some effect on the dynamic of the vehicle, whereas their effect on the rotational dynamics is small as compared to the translational dynamics.

In addition, it must be noted that this vehicle was operated along rail of the rig with some pitching effect during the experiment, and therefore the pitching may increases the experimental values as compared to the CFD results. This can be seen in the slight increase over the CFD results in Table 1. Besides, the movements of this vehicle are expressed by defining the relative velocity profile to the vehicle on the boundary. The C language programs were compiled to describe the velocity profiles, and these were then linked to the computation models via the user-defined function port of the software. The process can be quite slow and cause problem such as incorrect velocity transmitted to the AUV.

To further verify the CFD and experiment results, comparison with available data in literature based on computation and semi-empirical formulae for geometries of comparable shapes are useful to perform. Many of the available empirical relation provide only the linear damping coefficients, which are presumed to hold good for small value of angle attack or in this case the pitch angle (defined as the angle between velocity and longitudinal axis of the body) for the ROV but not for the AUV which moves at a larger pitch angle during diving (although the current study assumed zero pitching due to the current AUV design limitation). However, the present computations show that the nature of these forces and moments are essentially nonlinear and therefore for adequate representation for these forces and moments, a linear model is insufficient even over a small-velocity range. The geometry in the literature [White, 1977] has been used in this study. The model is axisymmetric with diameter, a hemispherical nose and a sinusoidal stern with tail radius 0.1 of the diameter. However, the AUV used in this study has no stern radius and the results can be different.

Moreover the available data on hydrodynamic coefficients for submerged vehicles is extremely scarce in literature [Tyagi and Sen, 2006; Tang et al., 2009]. Hence, a direct comparison of the computed derivatives with available results could be difficult. It can only be said that the estimated coefficient values presently are at best accurate within some bound. Since the main objective of the present work is to show that the CFD results are within the acceptable range and more importantly to show that CFD results essentially predict the forces or moments as nonlinear variation of the velocity using the same model. In this case, the Kempf model in [White, 1977; Tyagi and Sen, 2006] with L/D=6 is used. As shown in Table 1, the results seem to be higher than the one stated in the literature. This may be due to the boundary, meshing, outflow and inflow settings in the software that are not mentioned in the paper. However, the results exhibit around 5% error as compared to the results from the literature.

Finally, xPC Target software and hardware (see Fig. 11) were used to model, simulate and compare the hydrodynamic coefficients obtained from the semi-predictive method. The respective thrust inputs 1.2N (0.3m/s), 2N (0.5m/s) and 3.8N (0.95m/s) are used in these simulations. xPC Target was used to simulate the horizontal dynamics of the AUV using the hydrodynamic parameters obtained. It generates the simulated time responses to compare with the real-time experiment results obtained from the respective sensors. The sway position or the deviation of the AUV from its longitudinal axis is indirectly computed via the heading angle. The compass that read the heading angle gives the output in ASCII format. In the simulation, a fixed-step solver was used and the simulation was run for 70s. Due to space constraints, the AUV moving at 0.95m/s is presented only. As seen in Fig. 12, there are some differences between the dynamic predicted by the equations of motion in (2) and the experiment results. It is expected since the horizontal equations of motion have been simplified based on the assumptions made in the equations. As observed in the plots, the time responses in x, y positions and yaw angle are quite oscillatory due to the top control surface tried to overcome the opposing drag force during the experiment in water. Nevertheless, the simulated hydrodynamic coefficients (obtained through the experiments and numerical methods) do provide a good representation of the overall dynamics of the vehicle in water. However, the hydrodynamic coefficients can be further improved by repeating the entire process till the error between the simulated and experiment are small.

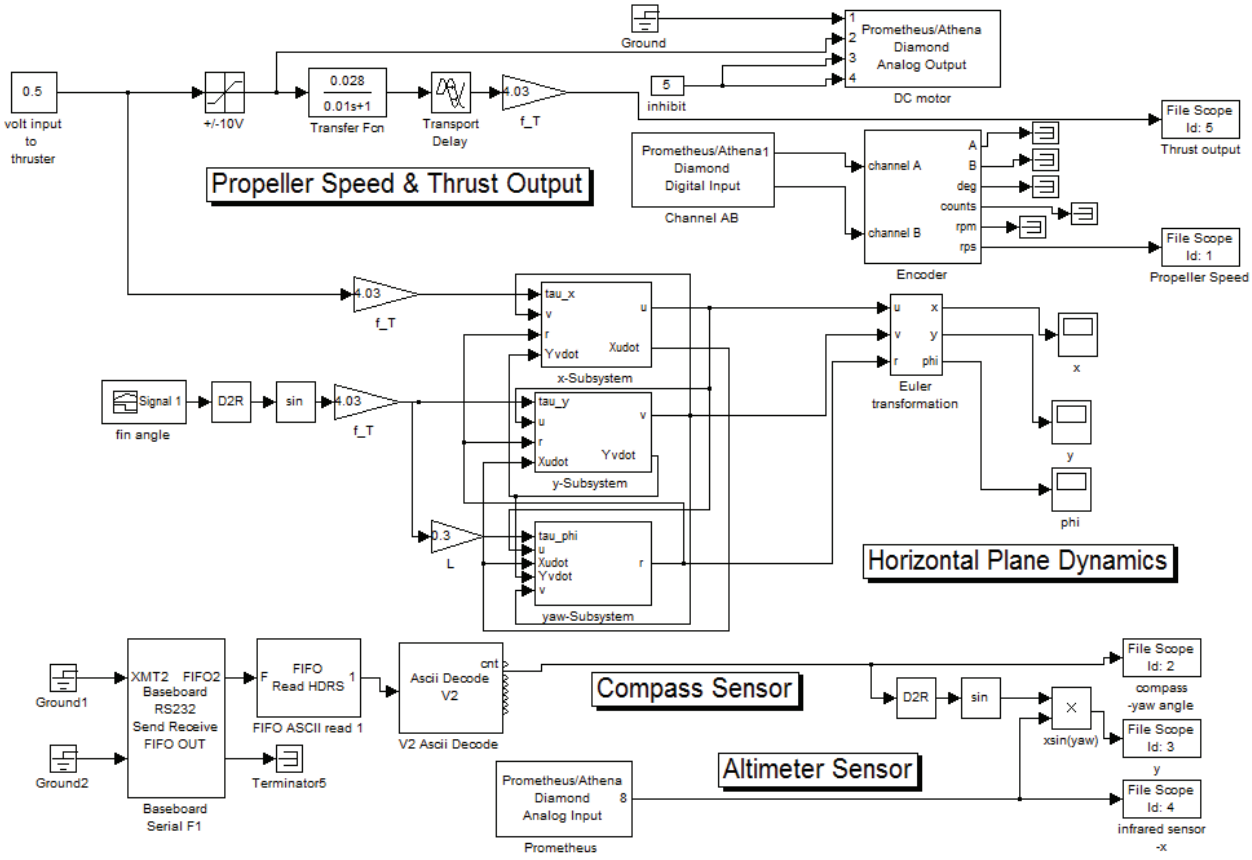

Figure 11: xPC Target in horizontal plane used in water tank test

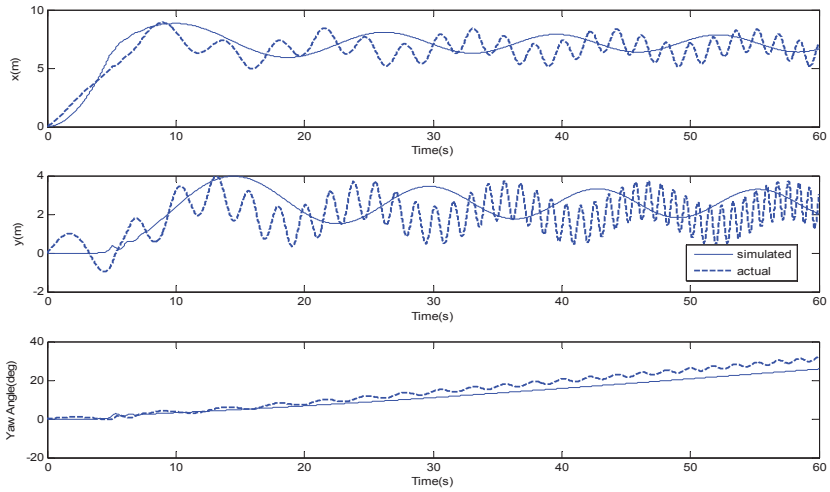

Fig. 12: Comparison between simulated vs actual in water tank at 0.95m/s

In summary, all of these findings offer a reference point for determining which coefficients need to be investigated when considering the proposed AUV that has a different shape as compared to the streamlined semi-empirical or empirical model at different conditions. The values of the parameters obtained for the AUV are tabulated in Table 2.

Descriptions	Values
D_a	0.25m
L	0.60m
m	14 kg
I_r	0.093 kg.m^2
$Y_{\dot{v}}$, $Y_{\|v\|v}$	29.4, $1.05N.m^{-2}s^2$
$N_{\dot{r}}$, $N_{\|r\|r}$	0.1, $1.04N.m^{-2}s^2$
$X_{\dot{u}}$, $X_{\|u\|u}$	1.4, $0.75N.m^{-2}s^2$

Table 2: Measured values for test-bed AUV

With the hydrodynamic parameters obtained in horizontal plane, the dynamics (denoted by subscript 'h') in (2) can be written in compact form:

$$\mathbf{M_h}\dot{\mathbf{v}}_\mathbf{h} + \mathbf{C_h}(\mathbf{v_h})\mathbf{v_h} + \mathbf{D_h}|\mathbf{v_h}|\mathbf{v_h} = \boldsymbol{\tau}_\mathbf{h} \tag{9}$$

where $\boldsymbol{\eta}_\mathbf{h} = [x \quad y \quad \psi]^{\mathrm{T}}$, $\mathbf{v_h} = [u \quad v \quad r]^{\mathrm{T}}$, $\boldsymbol{\tau}_\mathbf{h} = f_T\mathbf{T}\,\bar{\mathbf{u}} = [\tau_{xt} \quad \tau_{yt} \quad \tau_{\psi t}]^{\mathrm{T}}$ and φ is the angular position of the top control surface.

$$\mathbf{M_h} = \begin{bmatrix} m - X_{\dot{u}} & 0 & 0 \\ 0 & m - Y_{\dot{v}} & 0 \\ 0 & 0 & I_r - N_{\dot{r}} \end{bmatrix}; \mathbf{C_h}(\mathbf{v_h}) = \begin{bmatrix} 0 & (Y_{\dot{v}} - m)r & 0 \\ 0 & 0 & (m - X_{\dot{u}})u \\ 0 & -(Y_{\dot{v}} - X_{\dot{u}})u & 0 \end{bmatrix};$$

$$\mathbf{D_h} = \begin{bmatrix} X_u & 0 & 0 \\ 0 & Y_v & 0 \\ 0 & 0 & N_r \end{bmatrix}; \boldsymbol{\tau}_\mathbf{h} = \begin{bmatrix} 1 & 0 & 0 \\ 0 & \sin\varphi & 0 \\ 0 & 0 & L/2.\sin\varphi \end{bmatrix} f_\mathbf{T}\bar{\mathrm{u}}$$

6. Sliding-Mode Controller Design

To reduce the oscillation response of the top control surface as seen in the open-loop test, a closed-loop control system is required. The surge position is controlled by the propeller speed (using the PID controller) while the heading angle is controlled by the top control surface angle (denoted by φ). There have been various efforts to develop the controller for the AUV, which include both the linear, intelligent and robust control schemes. Given the complexities of is control requirements, it is clear that the linear controller is unable to control the vehicle satisfactorily [Yoerger et al., 1990]. Intelligent control methods which include neutral networks (NN), sliding mode (SLC) and fuzzy logic controllers (FLC) are more robust and able to adapt to the vehicle's hydrodynamic uncertainties. In addition, they exhibit excellent immunity to disturbances. For a start, the sliding mode controller [Utkin, 1977] is chosen to compensate for the modelling errors and uncertainties. By using xPC Target blocksets, the complex sliding mode control scheme can be easily implemented on the underwater robotic vehicle platform. For notational simplicity, define a scalar measure of tracking

$$s = \dot{\tilde{\varphi}} + \lambda\tilde{\varphi} \tag{10}$$

where $\tilde{\varphi} = \varphi - \varphi_d$ is the tracking angle error that is the error of the top control surface angle. $\lambda > 0$ is the control bandwidth. For $s = 0$, this expression describes a sliding surface with exponential dynamics

$$\tilde{\varphi}(t) = \exp[-\lambda(t - t_0)]\tilde{\varphi}(t_0) \tag{11}$$

which ensures that the tracking error $\tilde{\varphi}(t)$ converges to zero in infinite time when $s = 0$ (sliding mode). The error trajectory reaches the time-varying sliding surface in finite time for any initial condition $\tilde{\varphi}(t_0)$, and then slide along the surface toward $\tilde{\varphi}(t) = 0$ exponentially. Hence, the control objective is reduced to finding a control law which ensures that $\lim_{t\to\infty} s(t) = 0$.

In the design of the sliding control law, it is convenient to define a virtual reference φ_r satisfying

$$\dot{\varphi}_r = \dot{\varphi}_d - \lambda\tilde{\varphi} \Rightarrow s = \dot{\varphi} - \dot{\varphi}_r \tag{12}$$

Hence, the following expression for $\tau_m\dot{s}$ is obtained.

$$\begin{aligned} \tau_m\dot{s} &= \tau_m(\ddot{\varphi} - \ddot{\varphi}_r) \\ &= (K_m V - \dot{\varphi}) - \tau_m\ddot{\varphi}_r \\ &= -|\dot{\varphi}|s + (K_m V - \tau_m\ddot{\varphi}_r - |\dot{\varphi}|\dot{\varphi}_r) \end{aligned} \tag{13}$$

Consider the scalar Lyapunov-like function candidate

$$V_L(s,t) = \frac{1}{2}\tau_m s^2, \tau_m > 0 \tag{14}$$

Differentiating V_L with respect to time (as $\dot{\tau}_m = 0$) yields

$$\dot{V}_L = \tau_m s\dot{s} = -|\dot{\varphi}|s^2 + s(K_m\tau_\psi - \tau_m\ddot{\varphi}_r - |\dot{\varphi}|\dot{\varphi}_r) \tag{15}$$

Taking the control law for the top fin control surface to be

$$\tau_{\psi,s} = -1/K_m(K_d s + K\,\mathrm{sgn}(s)) \tag{16}$$

yields

$$\dot{V}_L = -|\dot{\varphi}|s^2 + s(-K_d s - K\,\mathrm{sgn}(s) - \tau_m \ddot{\varphi}_r - |\dot{\varphi}|\dot{\varphi}_r) \tag{17}$$

Conditions on the switching gain K_d and K are found by ensuring that $\dot{V}_L \le 0$. The particular choice

$$K_d + K \ge \tau_m \ddot{\varphi}_r + |\dot{\varphi}|\dot{\varphi}_r \tag{18}$$

where $\tau_m = 0.01$, and as the motor is intended to operate slowly, $\dot{\varphi}$ and $\dot{\varphi}_r$ become small. This implies

$$\dot{V}_L \le -(|\dot{\varphi}| + K_d)s^2 - K\,\mathrm{sgn}(s) \le 0 \tag{19}$$

Note that, $\dot{V}_L \le 0$ implies that $V_L(t) \le V_L(0)$, and therefore s is bounded. This in turn implies that $\ddot{V}_L$ is bounded. Hence $\dot{V}_L$ must be uniformly by continuous. Finally, application of Barbalat's lemma, then shows that $s \to 0$ and thus $\tilde{\varphi} \to 0$ as $t \to \infty$.The chattering can be eliminated by smoothing out the control law discontinuity inside a boundary layer by replacing the sign(.) function in the control law with sat(.). This substitution assigns a low-pass filter structure to the dynamics of the sliding surface inside the boundary layer.

By using xPC Target blocksets, the complex sliding mode control scheme can be easily implemented on the underwater robotic vehicle platform. The sliding mode control law in (17) is implemented as shown in Fig. 14. When the tracking error is negative (positive), indicating that the position is too small, the control input is increased (decrease) in order to increase the output. The "energy" of the system will diminish slowly as it reaches the sliding surface (near to zero tracking error). To test the robustness of the controller against the external disturbance, a low-frequency (2 Hz and having peak-to-peak amplitude less than 5) sine wave disturbance was injected into the system. The value of the external disturbance can be observed from the open-loop test where the top control plane oscillates no more than 5 degrees from its initial position. The passive approaches for the sliding mode control require it to be designed off-line in order to achieve the robustness against this disturbance. The control gains were adjusted to achieve the desired output during the simulation stage.

Once the robust controller is designed and simulated, the 10% model uncertainties (by decreasing and increasing the hydrodynamic coefficients by 10%) due to the sensitivity [Sen, 2000] of the model parameters on the vehicle response was implemented in xPC Target block diagram as shown in Fig 14. To compare the sliding-mode controller with other control scheme, few controllers are compared. Besides using PID controller to control the top control surface angular position in water, a linear quadratic regulator (LQR) was used. The controller gain for the LQR was calculated and implemented as a feedback gain. As shown in Fig. 13, the oscillatory motion has decreased. The steady state error using the sliding-mode controller seems to be smaller as compared to the PID and LQR controller. The robustness property of sliding-mode control can thus compensate the disturbances, in this case, the oscillatory behavior of the top control plane and the model uncertainties. With the results obtained in the hardware-in-the-loop testing, the proposed sliding-mode controller will be used in subsequent pool test. To verify the proposed rapid control systems prototyping using the xPC Target systems, the AUV was tested in the pool. Since the top and bottom control surface are connected and aligned to each other, the bottom control surface is used effectively to change the heading of the AUV while the top control surface to show the angular position of the fins in water. With the present sensors and system limitation, the application on an obstacle avoidance task seems to be appropriate for the AUV to perform.

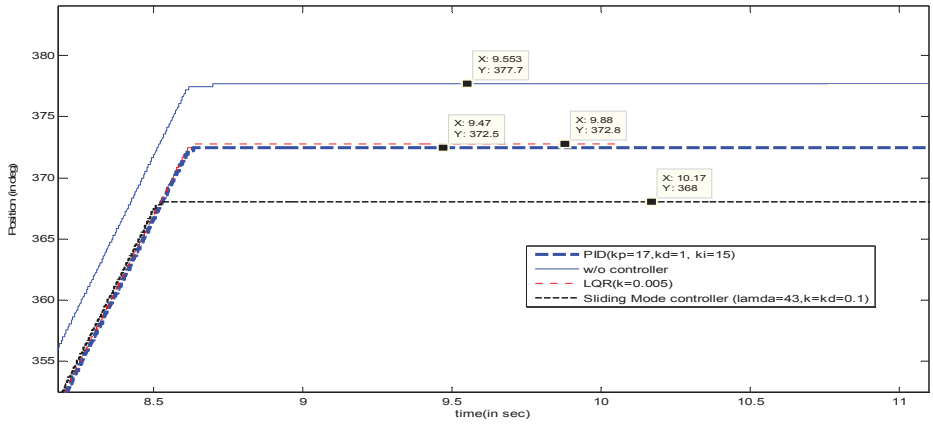

Figure 13: Time response of various controllers for certain angle

7. Experimental Pool Test for AUV

The block diagram used for the pool test is shown in Fig. 14. The propeller's speed was controlled by a PID controller. The sliding-mode controller was selected to control the angular position of the control surface. After the obstacle ("high" TTL signal equivalent of 2V) was detected, it sends a 5V to enable the fins' motor to rotate counter-clockwise (CCW). When the heading angle reads 90 degrees or more, the fins' motor rotates clockwise (CW) to its original position till the vehicle registers the 90 degrees heading angle. With the control algorithm finalized, the AUV was tested in the swimming pool as shown in Fig. 15. As seen in pool test, the motion of the AUV is now emulated in the pool environment. Initially, the AUV was positioned facing the wall of the pool as indicated by the arrow. The front wall facing the AUV was the obstacle to be avoided. The distance from the AUV to the pool's wall was around 2m. Once the 2m (or the wall) was reached, it began to make a 90 degrees turn to avoid the obstacle (as shown in the sequence 2 onwards in Fig. 15).

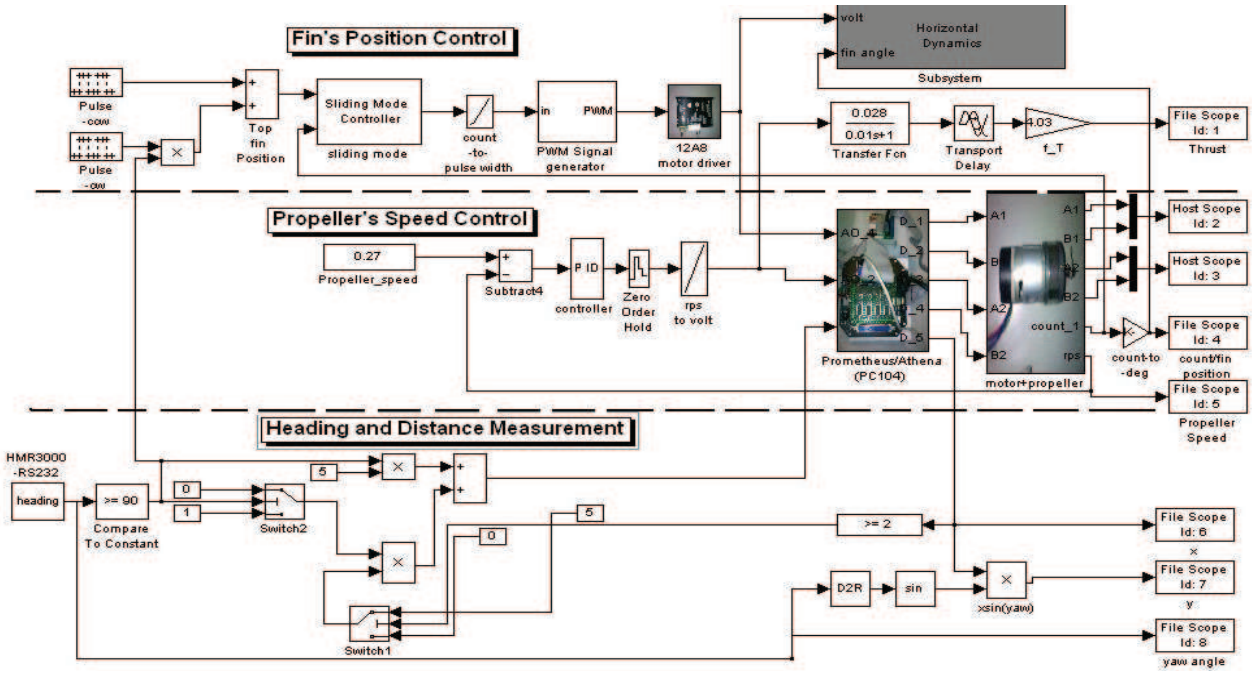

Fig. 14: xPC Target block diagram for obstacle avoidance

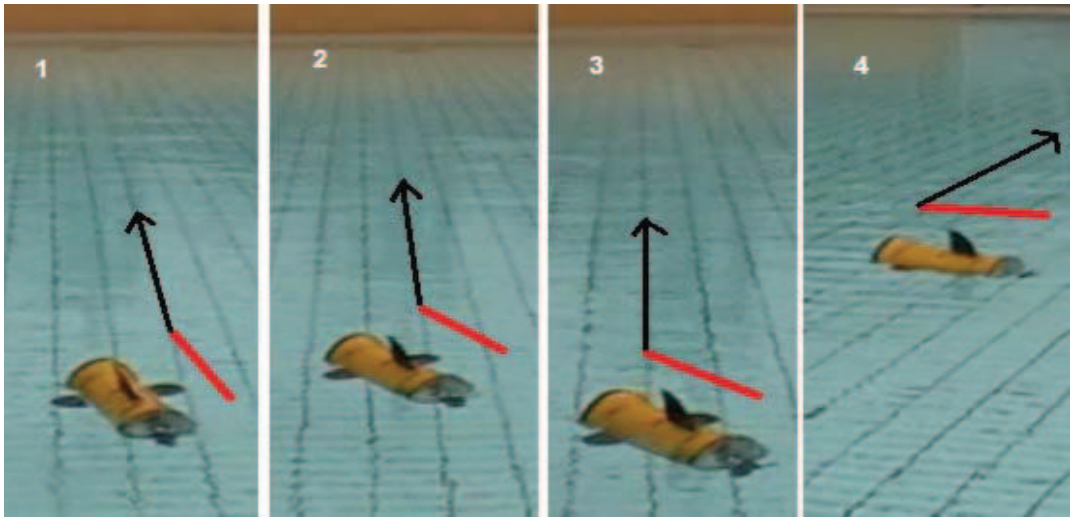

Figure 15: Actual motion sequence of AUV during obstacle avoidance in pool

The actual and simulated responses of the AUV in the pool are shown in Fig. 16. The obstacle was first detected at around 18s while maneuvering at a slow propeller's speed of 0.27 rps. The top control surface started to rotate CCW until the heading angle registered 90 degrees to rotate CW. As shown, the top control surface angular position exhibits less oscillation as compared to the open-loop case. The simulated responses of the x, y and yaw angle from the horizontal plane model were compared with the actual measurement obtained though the sensors. The simulated transient behavior is found to be different as compared to the experiment results. It can be due to the initial water resistant that the AUV needs to overcome. However it is quite negligible for this case.

On the other hand, the x, y positions response are quite oscillatory with some overshoot. However, with the sliding-mode controller, it managed to achieve the steady-state value at around 20s. The resistance force could increase if the angular position of the top control surface increases. After many trials to decrease the resistance, the top control surface angles were set to 10 degrees, to achieve the desired AUV's heading direction with least resistance. In summary, the angular position of the top control surface was successfully controlled with least oscillation and the simulated results in both the positions and the heading angle match the actual experiment results in the pool. As observed in the pool test, despite of the model uncertainties such as the hydrodynamic parameters, and some spouting water, the AUV was able to perform and behave quite close to the simulated model.

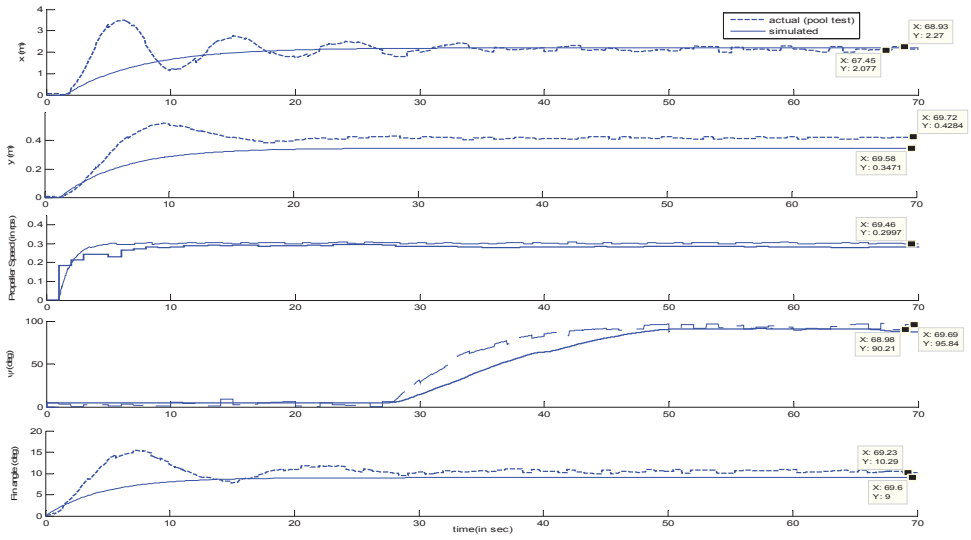

Fig. 16: Time responses of AUV during obstacle avoidance in pool

8. Conclusion

A systematic approach to rapid control system prototyping for the autonomous underwater vehicle (AUV) was implemented using the software xPC Target software and the hardware. The steady state thruster's model was obtained to establish the relationship between the voltages, speeds and thrusts output. The horizontal plane dynamic including the nonlinear hydrodynamic damping of the AUV was determined through the water tank test using xPC Target software and hardware, and later verified with ANSYSY CFX numerically. The sliding mode controller was able to control the top control surface angle during the heading maneuvering in the pool trials under the disturbances. As for the future works on the modelling aspects of the AUV parameters, the accuracy or sensitivity of the hydrodynamic coefficients estimated in this study can be improved by using the GPS antenna, ballast releaser, obstacle detection sonar, and transponder (SSBL). The sea trial will be conducted with the use of a global positioning system to provide a real-time position of the vehicle. Besides, as seen in the simplicity of the AUV design, the proposed xPC Target can also be used in the computer-aided engineering education.

Acknowledgment

This work was made possible by support of Temasek Polytechnic and technical guidance from MathWorks. The authors appreciate the valuable technical support from the staff and students throughout the project.

References

[1] Milam W, P. A.,1993. Distributed computing approach to rapid prototyping for embedded controllers. Proceedings of the 36th Midwest Symposium on Circuits and Systems, Detroit, MI, USA, 2, 1155–1158.

[2] Hanselmann, H., 1996. Automotive control: from concept to experiment to product. Proceedings of the 1996 IEEE international Symposium on Computer-aided Control systems design, Dearborn, Michigan, USA, 129–134.

[3] Burns, D., Sugar, T., 2002. Rapid embedded programming in the mathworks environment. ASME Journal of Computing and Information Science Engineering, 2(3),237–241.

[4] Chen, C. Y., Shun, Y. C., Cheng, C. C., Liao, P. S., Fang, Z. C., 2007. MATLAB-based Rapid Controller Development Platform for Control Application. Proceedings of the Institution of Mechanical Engineers, Part C: Journal of Mechanical Engineering Science, 221(11), 1461-1473.

[5] Loh, R. N. K., Pornthanomwong, T., Pyko, J. S., Lee, A., Karsiti, M. N., 2007. Modelling, Parameters Identification, and Control of an Electronic Throttle Control (ETC) System. International Conference on Intelligent and Advanced Systems, Kuala Lumpur, Malaysia, 1029-1035.

[6] Chu, L., Fang, Y., Shang, M. L., Guo, J. H., Wei, W. R., Liu, M. H., Li, J., 2009. Development of test bench for integrative evaluation of the pneumatic ABS/TCS performance. 5th IEEE Conference on Vehicle Power and Propulsion, Dearborn, Michigan, USA, 1079-1084.

[7] Guo, H. Y., Chen, H., Song, T. H., 2009. Tire-road forces estimation based on sliding mode observer. International Conference on Mechatronics and Automation, San Diego, California, USA, 4577-4582.

[8] Saad, N., Zailani, M. S. R., 2007. Industrial PC control implementation on PID controllers: application to pressure control system, International Conference on Intelligent and Advanced Systems, Kuala Lumpur, Malaysia, 1007-1012.

[9] Adnan, B. M., Nordin, S., Ismail, I., Baloch, T. M., Hanif, N. H., Mohamad, N. H. H., 2010. Design and analysis of PI-Fuzzy controller for temperature control system. Proceeding of 2010 Fourth Asia International Conference on Mathematical/Analytical Modelling and Computer Simulation, Kota Kinabalu, Borneo Island, Malaysia, 378-383.

[10] Park, C. H., Choi, S. K., Son, Y. S., Han, Y. H., 2009. Development of 5kWh flywheel energy storage system using MATLAB/xPC Target. Proceeding of 2009 WRI World Congress on Computer Science and Information Engineering, Los Angeles, California, 2, 701-705.

[11] Fei, Y., Yang, Y.,2006. Optimal vibration suppression of a flexible structure using piezoceramic actuators. In: Proceeding of SSST '06 Southeastern Symposium on system Theory, Cookville, USA, 10–13.

[12] Low, K. H., Wang, H., Wang, M. Y.,2005. On the Development of a Real Time Control System by using xPC Target: Solution to Robotic System Control. Proceedings of the 2005 IEEE International Conference on Automation Science and Engineering, Edmonton, Canada, 345-350.

[13] Wei, Y. J., Patton, J., Bajaj, P., Scheidt, R., 2005. A real-time haptic/graphic demonstration of how error augmentation can enhance learning. In: Proceedings of 2005 IEEE International Conference on Robotics and Automation, Barcelona, Spain, 4406-4411.

[14] Chin, C. S., Lau, M. W. S., Tan, Y. J., Chee, K. F., Wong, Y. C., 2009. Development and testing of an autonomous underwater vehicle using industrial xPC Target platform. Proceeding of IEEE/ASME International Conference on Advanced Intelligent Mechatronics, Singapore, 1076-1081.

[15] Fehrani, H., Heidari, N., Zakeri, M., Ghaisari, Y., Jafar, 2010. Development, depth control and stability analysis of an underwater ROV, 8th International Conference on Control and Automation, Xiamen, China, 814-819.
[16] Byron, J., Tyce, R., 2007. Designing a vertical/horizontal AUV for deep ocean sampling. OCEAN 2007, Vancouver, Canada, 1-10.
[17] Ura, T., Nakatani, T., Nose, Y., 2006. Terrain-based localization method for wreck observation AUV. In: Proceedings of OCEANS, Boston, USA, 1–6.
[18] Utkin, V. I., 1977. Variable structure system with sliding modes. IEEE Transactions on Automatic Control, 22(2), 212–222.
[19] Fossen, T. I., 2002. Marine Control Systems: Guidance, Navigation and Control of Ships, Rigs and Underwater Vehicles, second ed. John. Wiley, Chichester.
[20] Gertler, M., Hagen, G., 1967. Standard equations of motion for submarine simulation. David Taylor Naval Ship Research and Development Center, Tech. Rep., Defense Tech. Inform. Center Doc, 653 861.
[21] Lamb, S. H., 1932. Hydrodynamics. Cambridge University Press, Cambridge.
[22] Aage, C., Wagner, L.S., 1994. Hydrodynamic manoeuvrability data of a flatfish type AUV. Proceedings of OCEANS 1994, 3, 425–430
[23] Yoon, H. K., Son, N. S., Lee, C. M., 2007. Estimation of the roll hydrodynamic moment model of a ship by using the system identification method and a free running model test. IEEE J Ocean Eng. 32(4),798–806
[24] Yoon, H. K., Son, N. S., 2004. Estimation of roll-related coefficients of a ship by using the system identification method (in Korean). J Soc Naval Archit Korea, 41(4),53–58
[25]Jones, D. A., Clarke, D.B., Brayshaw, I.B, 2002. The calculation of hydrodynamic coefficients for underwater vehicles. DSTO Platforms Sciences Laboratory, Fishermans Bend, Australia, Report. DSTO-TR-1329
[26] Nahon, M., 1993. Determination of undersea vehicle hydrodynamic derivatives using the USAF DATCOM. Proceedings of OCEANS, 2, Victoria, 283–288.
[27] Humphreys, D.,1981. Dynamics and hydrodynamics of ocean vehicles, Proceedings of OCEANS, 13, 88–91.
[28] Kim, K., Kim, J., Choi, H. S., 2002a. Estimation of hydrodynamic coefficients of a test-bed AUV-SNUUV1 by motion test, Proceedings of OCEANS, 1, 29–31, 186–190.
[29] Kim, J., Kim, K., Choi, H. S., 2002b. Estimation of hydrodynamic coefficients for an AUV using nonlinear observers. IEEE J Ocean Eng , 27(4), 830–840.
[30] Whitcomb, L. L., Yoerger, D. R., 1999. Development, comparison, and preliminary experimental validation of nonlinear dynamic thruster models. IEEE Jounal of Ocean Engineering, 24 (4), 481–494.
[31] Yoerger, D. R., Cooke, J. G., Slotine, J. J. E., 1990. The influence of thruster dynamics on underwater vehicle behavior and their incorporation into control systems design. IEEE J. Ocean. Eng., 15 (3), 167–178.
[32] White, N. M., 1977. A comparison between a single drag formula and experimental drag data for bodies of revolution, DTNSRDC Report 77-0028.
[33] Tyagi, A., Sen, D., 2006. Calculation of transverse hydrodynamic coefficients using computational fluid dynamic approach. Ocean Eng, 33(5–6), 798–809.
[34]Tang, S., Ura, T., Nakatani, T., Thornton, B., Jiang, T., 2009. Estimation of the hydrodynamic coefficients of the complex-shaped autonomous underwater vehicle TUNA-SAND. Journal of Marine Science Technology, 14, 373-386.
[35] Sen, D., 2000. A study on sensitivity of manoeuvrability performance on the hydrodynamic coefficients for submerged bodies. J Ship Res, 45(3), 186–196.